Linear MPC for anesthesia process with external predictor

A. Pawłowski[1], **M. Schiavo**[2], **N. Latronico** [3], **M. Paltenghi**[4], **A. Visioli**[1]

[1]*Dipartimento di Ingegneria Meccanica e Industriale, University of Brescia, Brescia, Italy*
andrzej.pawlowski@unibs.it, antonio.visioli@unibs.it

[2]*Dipartimento di Ingegneria dell'Informazione, University of Brescia, Brescia, Italy*
schiavo003@unibs.it

[3]*Department of Surgery, Radiology, and Public Health, University of Brescia, Italy*
nicola.latronico@unibs.it

[4]*Spedali Civili di Brescia, Brescia, Italy*
massimiliano.paltenghi@asst-spedalicivili.it

This is the pre-print version of the following article: Linear MPC for anesthesia process with external predictor, which has been published in final form at 110.1016/j.compchemeng.2022.107747.

Abstract: In this paper we present a new model predictive control system for the depth of hypnosis in general anesthesia. The depth of hypnosis is measured by the Bispectral Index Scale signal and controlled through propofol administration. The proposed control scheme is based on an external predictor that, by exploiting the Wiener structure of the pharmacokinetic/pharmacodynamic model of propofol, compensates for the process nonlinearity and increases the system robustness by means of an additional filter. The performance of the developed control scheme is evaluated through an extensive simulation study, which considers inter-patient and intra-patient variability by applying a Monte Carlo technique. The obtained results show that the proposed methodology is effective in both the induction and maintenance phases.

1. Introduction

Automated systems for drug delivery have attracted the attention of the control system community due to the presence of challenging issues such as nonlinearities and variable time delays, variable dynamics for specific drug/agent administration, robustness related to the patient safety [1–3]. In this context, a significant effort has been made for systems that use feedback control concepts to develop automatic regulation schemes of physiological variables like blood pressure, blood glucose concentrations, etc. [4]. In particular, general anaesthesia process plays an important role in intensive care and in many surgical interventions with a significant potential to be supported by an automatic control system. The main goal of the anaesthesia process regulation is to assure the required level of analgesia, muscle relaxation and depth of hypnosis (DoH) through the administration of specific drugs [2, 4, 5].

In this work we focus on the control system for depth of hypnosis. In the typical clinical practice, anesthesiologists manually adjust the propofol administration basing on their professional experience and on the available patient's vital signs, including Bispectral Index Scale (BIS), which indicates the DoH level. Due to the great variability in the patient's response to the drug, even experienced professionals may commit errors, with the result of either an under- or an over-estimation of the required propofol dosage. In case of underdosing, the patient might regain consciousness during the surgery and potentially experience trauma. Conversely, propofol overdosing can lead to undesired effects on the patient in the form of arterial hypotension and post-operative delirium [6]. In light of these possible pitfalls, it is desirable to develop automated drug dosing techniques to prevent under or overdosing issues and to provide a more adapted solution.

The development of a reliable control system for DoH has been attracting the attentions of the automatic control research community for a few decades [4]. This challenging control problem has been analyzed from different

control techniques points of view. The common goal consists of providing a control strategy that supports anaesthesiologists in their clinical practice and that is suitable for a vast population of patients by satisfying the highest medical safety requirements. In the design of the control system, the main problems to consider are related to the existence of a strong process nonlinearity and of inter- and intra-patient variability [4, 7, 8].

For this reason, many control approaches have been devised. Most of them can be divided into two main groups depending on the controller type [4, 9].

In the first group a PID (Proportional-Integral-Derivative) controller is used and its tuning to satisfy clinical requirements is primarily addressed [4, 10–19]. Additionally, adaptive control architectures are build on this classical feedback controller [20]. Moreover, this classical approach can be also extended with a feedforward controller to improve the control system response [6, 21]. Nevertheless, the main drawback of PID-based control systems for DoH is their lack of the constraints handling mechanism and their inability to anticipate the response of the patient drug metabolism. For this reason, they frequently yield a sub-optimal performance.

The second group is based on model predictive control (MPC) techniques, which exploit the nominal pharmacokinetic/pharmacodynamic (PK/PD) patient model for control purposes. Indeed, they allow DoH process constraints to be directly defined into the cost function that is used for determining the control signal. The application of MPC techniques to the anaesthesia process has been analyzed in several works. Most of them use a state estimator (such a Kalman filter [1, 22]), which might yield a large settling time. In [7, 23] a piece-wise linearization of the Hill function is proposed to eliminate the nonlinear component from the control loop. The control scheme, then, uses a hybrid multi-parametric-MPC (mp-MPC) approach. The computation of the control signal requires the usage of computationally costly solvers, like multi-parametric Mixed Integer Quadratic Programming (mp-MIQP) or multi-parametric Quadratic Programming (mp-QP) for a simplified control approach. Another approach based on a mp-MPC has been proposed in [8, 24], where the controller is coupled with an external estimator exploiting two methods, a Kalman filter and an online/offline moving horizon, used to address the inter- and intra-patient variability. Additionally, the inverse of the static nonlinearity is used to linearize the system. This compensation of the PK/PD model nonlinear element and the application of a linear MPC is also proposed in [25]. In particular, the Extended Prediction Self-Adaptive Control (EPSAC) algorithm is used. The proposed controller exploits the clipping technique by limiting the control horizon up to one sampling instant, with the result of a limited tuning and, as a consequence, of a sub-optimal performance. Moreover, due to the clipping technique, the predictive controller does not take into account constraints when computing the optimal control signal for the process. They are applied *a posteriori* when the computed signal violates the saturation limits.

The control system proposed in [26] also uses the inverse of the nonlinear part of the pharmacodynamic model to linearize the process. Different approaches for propofol chemo-dynamics, taking into account a time delay, are considered. The main issue analyzed concerns the mismatch in time delays between the used model and the patient. Obtained results from the clinical trial show that an MPC-based system can be effective in DoH control in general anaesthesia.

In any case, it appears that there is still the need to provide simple and efficient MPC strategies that can be suitable to be applied in practice and whose the robustness is clearly demonstrated. Extending a PID-based approach presented in [17],in this paper we propose to use a novel control architecture based on the Generalized Predictive Control (GPC) algorithm to handle all the constraints. The GPC controller is widely used in many industrial process control applications due to its efficacy and adaptability [27, 28], but, with respect to the previously mentioned MPC techniques, here the Wiener PK/PD model is applied straightforwardly and it is integrated within the control scheme. In this way, we avoid a complex design of the state estimators and we provide an easily implementable and efficient solution that achieves a suitable trade-off between the model complexity and the accuracy of the real patient response approximation. Moreover, the control system design is performed basing on the physical patient parameters, which are used for defining the employed model. In fact, the linear component of the Wiener model used for the controller design is obtained separately for each individual while the patient model nonlinearity is compensated by inverting the one of the average patient, since it cannot be estimated for each individual. The linear model is used as a predictor, while a low-pass filter is employed for the attenuation of the differences between the model and the real patient responses. This filter provides an extra degree of freedom in the control system and is designed for performance adjustment. Additionally, a reference filter leads to the achievement of the desired performance in the induction phase. Thus, a two-degree-of-freedom controller is obtained [18, 29]. Due to this configuration, the controller and the filter need a simultaneous co-design, which is performed using a genetic algorithm. Then, the robustness of the system is verified through an extensive inter- and intra-patient variability analysis with a Monte Carlo method.

The paper is organized as follows: Section 2 briefly reviews the PK/PD model of propofol used in the control scheme. Section 3 describes the proposed control architecture for the DoH, the GPC algorithm and the tuning procedure. Section 4 presents the results of the control approach tested in the simulation for induction and maintenance phases. In addition, inter- and intra-patient variability analysis is shown as well as a comparison with other

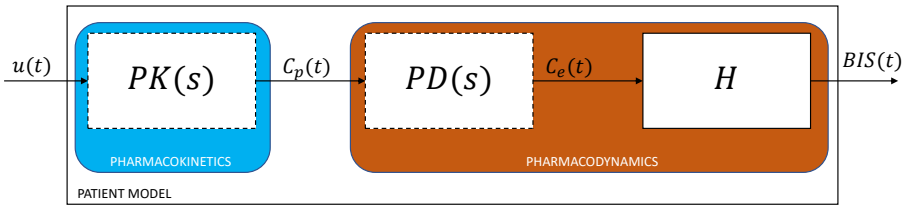

Fig. 1: Schematic representation on the patient PK-PD model for propofol dosage response.

control systems. Finally, conclusions are given in Section 5.

2. Pharmacokinetic-pharmacodynamic model of propofol

The BIS response to propofol adminstration is determined by using a realistic patient model based on PK/PD response to the drug infusion [30–34]. The PK refers to the infusion, distribution and elimination of the drug in the body, while the PD characterizes the relationship between the blood concentration of the drug and its clinical effect. The propofol effect on the human body can be represented using the linear PK dynamics connected in series with the PD dynamics, which is modelled by a linear part and a static nonlinear element as shown in Figure 1 (where the blocks representing linear dynamics are indicated with dashed lines).

The PK term describes a mamillary three compartmental model, where each compartment is homogeneous with uniform drug distribution. The input of the model $u(t)$ $[mg/s]$ represents the infusion rate of the drug, while the output of the PK term is the plasmatic concentration of the drug $C_p(t)$ and also the input of the PD term of the model. The resulting PK transfer function is:

$$PK(s) = \frac{C_p(s)}{U(s)} = \frac{1}{V_1} \frac{(s+z_1)(s+z_2)}{(s+p_1)(s+p_2)(s+p_3)} \tag{1}$$

where p_1, p_2, p_3, z_1 and z_2 depend on the characteristics of the patient (age, weight, height, gender) [6, 30, 34].

The linear part of the PD term considers a fictitious compartment called effect-site compartment and it is added to represent the lag between the plasma concentration and the corresponding drug effect. The drug concentration in the effect-site compartment is expressed as C_e, where $\dot{C}_e(t) = k_{1e}C_p(t) - k_{e0}C_e(t)$. In accordance with [30], the propofol transfer frequency k_{1e} is considered constant and equal to the frequency of drug removal from the effect-site compartment with $k_{1e} = k_{e0} = 0.456$ $[min^{-1}]$. The resulting PD transfer functions is:

$$PD(s) = \frac{C_e(s)}{C_p(s)} = \frac{k_{e0}}{s+k_{e0}} \tag{2}$$

Finally, a static nonlinear sigmoidal function, known as Hill function, correlates the effect-site drug concentration and the clinical effect, given by the BIS index [32, 35]. It can be written as:

$$BIS(t) = E_0 - E_{max}\left(\frac{C_e(t)^\gamma}{C_e(t)^\gamma + C_{e_{50}}^\gamma}\right), \tag{3}$$

where E_0 is the baseline value representing the BIS level of the patient in the initial state before the infusion, $E_0 - E_{max}$ is the maximum reachable effect achieved by the infusion, γ denotes the steepness of the curve that represents the receptiveness of the patient to the drug and $C_{e_{50}}$ is the necessary concentration of the drug to reach the half maximal effect.

The PK/PD model is therefore a Wiener model, where a linear model is connected in series with a static nonlinear function [30, 32, 36]. The linear component is obtained by multiplying the linear blocks of the PK and PD resulting in $P(s) = PK(s) \cdot PD(s)$.

3. Control scheme

3.1. Control specifications

The control structure of the DoH process exploits the patient BIS signal as feedback information and aims to reach and keep the desired DoH level by manipulating the propofol infusion rate. In the induction phase, the controller should bring the patient's level of hypnosis to the desired value within an established time interval. According to the clinical specifications, a reference BIS value of 50 has to be reached in about 120 $[s]$. Although this is not a

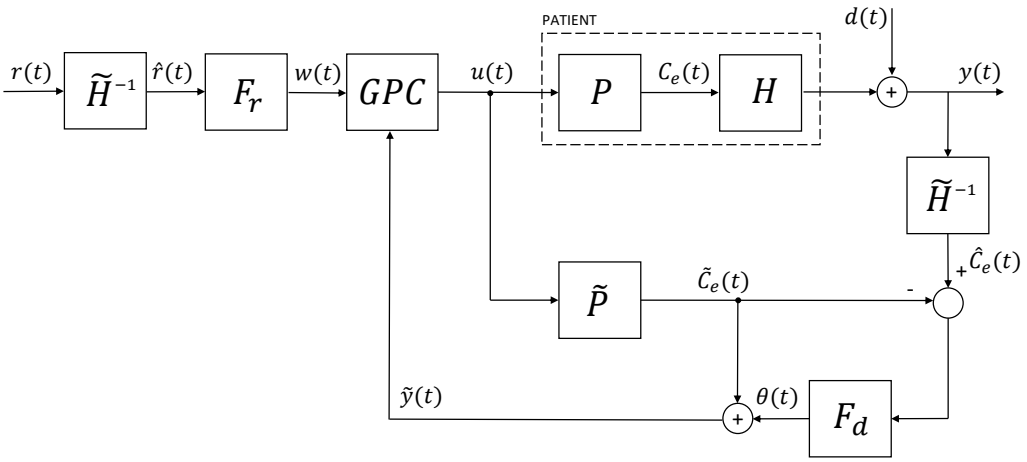

Fig. 2: The GPC-based control scheme with the external predictor.

strict requirement, it is mandatory that the reference be reached within 300 $[s]$ to avoid an excessive discomfort for the patient. In the maintenance phase, acceptable BIS values are between 40 and 60. The BIS value should be kept into this range despite the presence of disturbances due to nociceptive stimulations.

An additional specification to be considered concerns the minimum and maximum permissible infusion rates. The minimum value is obviously 0 $[mg/s]$ and corresponds to the non-infusion situation of the drug. The upper limit of the infusion rate has been set at 6.67 $[mg/s]$ for the induction phase and at 4.00 $[mg/s]$ for the maintenance phase. The first value has been obtained by considering the mechanical limit of the infusion device. In particular, we have considered the maximum infusion rate of 1200 $[ml/h]$ achievable by a commercially available medical pump (*Graseby 3400, Smiths Medical, London, UK*) and a standard concentration of the hypnotic drug propofol (*Diprivan* 20 $[mg/ml]$). On the other hand, the second value represents the maximum infusion rate typically used during a bolus in the maintenance phase when anesthesia is administered manually. The choice of using two different upper limits for the two phases of anesthesia is therefore in accordance to the clinical practice. Indeed, a higher infusion rate is appropriate during the induction phase since it is desirable to rapidly induce anesthesia in order to reduce patient's discomfort and to quickly secure the airway.

3.2. Control system architecture

The proposed control structure is shown in Figure 2. It integrates the PK/PD patient model and compensates its nonlinear part by inverting it. In fact, the GPC design and development (computation of internal matrices) are performed by taking into account the nominal linear part of the model based on the individual patient characteristics. In this way the available physical parameters of the patient are embedded into the used model.

Figure 2 shows that the patient is represented by the previously introduced nonlinear model, where the linear part P and the nonlinear part H can be distinguished. However, in practice, exact values for these two components are unknown and need to be calculated with an inaccurate PK/PD model. For this reason, in the compensator structure we refer to these elements as $\tilde{P}$ and $\tilde{H}$ for the linear and the nonlinear part, respectively, in order to distinguish them clearly from real ones. As already mentioned, $\tilde{P}$ can be obtained for each individual patient basing on their physiological data. Instead, since $\tilde{H}$ cannot be obtained for each individual patient, its value is computed by taking into account the average values of the parameters reported in literature [30–32], which are E_{max}=87.5, $C_{e_{50}}$=4.92, γ=2.69 and E_0 is the BIS signal value for the fully awake patient. The E_0 value can be measured before the induction phase and the correct value can be used for each patient. The $\tilde{P}$ block input signal $u(t)$ represents the propofol dosage rate and its output is the estimated effect site concentration $C_e(t)$ of the patient. To compensate the nonlinear behaviour present in the PK/PD model, the inverse of average Hill function $\tilde{H}^{-1}$ is introduced and defined as:

$$\tilde{H}^{-1} = C_{e_{50}} \sqrt[\gamma]{\frac{\bar{E} - E_0}{E_0 - \bar{E} - E_{max}}}$$

where $\bar{E}$ is the current BIS signal value. In the nominal case, when there are no modelling errors and uncertainties between the model and the patient, (namely, $\tilde{P} = P$ and $\tilde{H} = H$), the architecture can be converted to a linear control system of the linear component of PK/PD model. In the resulting control scheme, $w(t)$ is the filtered value of $\hat{r}(t)$, which is the reference value of the effect site concentration that reflects the desired BIS reference $r(t)$.

The $\hat{r}(t)$ value is computed using $\tilde{H}^{-1}$ that relates the BIS and the estimated effect site concentration $C_e(t)$ of the patient. Therefore, in the nominal case, $\hat{C}_e(t) = \tilde{C}_e(t)$ and the resulting feedback signal is equal to $\tilde{C}_e(t)$. This only changes when the controlled process output is affected by the disturbances $d(t)$.

In practice, model uncertainties are unavoidable, in particular those related to the static nonlinearity in the Wiener model. This is because it is virtually impossible to know the exact values of the parameters *a priori*. Additionally, the linear component of the PK/PD model has uncertainties owing to model inaccuracy and parameters variability. For this reason, the $\theta(t)$ signal will be used to compensate differences related to modelling uncertainties and for the disturbances induced by surgical stimuli. The contribution of $\theta(t)$ depends on the error between the estimated effect site concentration $C_e(t)$ and the effect site concentration $\hat{C}_e(t)$ calculated with the BIS signal via the average Hill function inversion. In this way, the $w(t)$ signal is used as the reference for the GPC controller, while the controlled variable is $\tilde{y}(t)$, containing information about patient model mismatch and disturbances (the feedback signal). The resulting contribution of the $\theta(t)$ signal is attenuated by the F_d filter, placed in the feedback loop, which reduces the effect of uncertainties and disturbances on the GPC controller and simultaneously guarantees a zero steady-state tracking error. The F_d filter will affect directly the response of the control signal to the disturbances and to the model uncertainties. Moreover, it will provide additional robustness since filtered disturbances are introduced into the control loop. We select F_d as a first-order low-pass filter:

$$F_d(s) = \frac{1}{T_d s + 1} \tag{4}$$

Additionally, in order to build a two-degree-of-freedom scheme, the F_r filter is used to achieve the desired set-point response, where the controller focuses on the disturbance rejection task. The F_r transfer function is:

$$F_r(s) = \frac{1}{T_r s + 1} \tag{5}$$

The resulting control system needs to be tuned with the typical two-degree-of-freedom methodology, where the controller and the F_d filter are first tuned by focusing on the disturbance rejection performance (maintenance phase). Then, F_r is adjusted to obtain the desired performance for the reference tracking task (induction phase).

3.3. Generalized Predictive Controller algorithm

As it is well known [27], GPC consists of applying a control sequence that minimizes a multistage cost function of the form:

$$J = \sum_{j=N_1}^{N} [\hat{y}(t+j|t) - w(t+j)]^2 + \sum_{j=1}^{N_u} \lambda [\Delta u(t+j-1)]^2 \tag{6}$$

where $\hat{y}(k+j|t)$ is an optimal system output prediction sequence performed with known data up to discrete time t, $\Delta u(t+j-1)$ is a future control increment sequence obtained from cost function minimization with $\Delta = (1 - z^{-1})$, N_1 and N are, respectively, the minimum and maximum prediction horizons, N_u is the control horizon and λ weights the future control efforts (with respect to the tracking errors) along the horizon. The horizons and weighting factor are design parameters used as tuning variables. The reference trajectory along the prediction horizon is represented by $w(k+j)$ [27]. In (6), the j-step ahead prediction of system output with data up to time t, $\hat{y}(k+j|t)$, is computed using the following model representation [27]:

$$A(z^{-1})\tilde{y}(t) = B(z^{-1})u(t-1) + \frac{e(t)}{\Delta} \tag{7}$$

where A and B are adequate polynomials in the backward shift operator z^{-1} and $e(t)$ is a zero mean white noise that is set equal to zero. The prediction equation in vectorial form can be expressed as:

$$\hat{\mathbf{y}} = \mathbf{G}\mathbf{u} + \mathbf{f}; \tag{8}$$

where $\hat{\mathbf{y}}$ are the future process outputs, $\mathbf{G}$ is the dynamics matrix, $\mathbf{u}$ are the control signal values (decision variable) and $\mathbf{f}$ are the values of the free response of the process (see [27] for more details).

3.3.1. Control signal constraints

The predictive controller is able to handle the constraints in the optimization procedure. This is an important feature from a practical point of view since all limitations are considered in computed control signal, which results in a better performance.

The limitations of the control signal described in Section 3.1 (given as $u_{min} = 0$ $[mg/s]$ and $u_{max} = 6.67$ $[mg/s]$

for the induction phase and $u_{max} = 4\ [mg/s]$ for the maintenance phase) have to be included into the optimization procedure. For this purpose, the saturation limits, $u_{min} \leq u(t) \leq u_{max}$ can be expressed as a function of inequalities on control signal increments:

$$\mathbf{l}u_{min} \leq \mathbf{T}\Delta\mathbf{u} + u(t-1) \leq \mathbf{l}u_{max}.$$

where $\mathbf{T}$ is $N \times N$ lower triangular matrix of ones, $\mathbf{l}$ is a $1 \times N$ vector of ones. The slew-rate constraints are imposed directly on the control signal increments vector Δu. In this case, the constraints can be expressed through the inequality $\Delta u_{min} \leqslant u(t) - u(t-1) \leqslant \Delta u_{max}$. As in the previous case, this can be rewritten in vectorial form as:

$$\mathbf{l}\Delta u_{min} \leqslant \Delta\mathbf{u} \leqslant \mathbf{l}\Delta u_{max}$$

The slew-rate constraints are also adjusted depending on the anaesthesia phase. In particular, we have $-1 \leqslant \Delta\mathbf{u} \leqslant 1$ in the induction phase $[mg/s]$, and $-0.4 \leqslant \Delta\mathbf{u} \leqslant 0.4\ [mg/s]$ in the maintenance phase.

In order to obtain a desired behaviour of the manipulated variable, it is also necessary to introduce additional constraints for the maintenance phase. In particular, if the sum of Δu in the last 5 samples is greater than 0.5, then the maximum allowed decrement of the manipulated variable (for the next calculation) is set to $\Delta u_{min} = -0.1$. This compensates for positive disturbances preventing the controller output to decrease too fast. Additionally, if the BIS value is lower than the reference, then the maximum allowed increment of the manipulated variable is set to $\Delta u_{max} = +0.1$. In this way, when there is a negative disturbance, the manipulated variable is forced to stay at low levels until the BIS reaches the reference.

These constraints can be expressed, in general, as $\mathbf{R}\Delta\mathbf{u} \leqslant \mathbf{c}$ where:

$$\mathbf{R} = \begin{bmatrix} \mathbf{I}_{N\times N} \\ -\mathbf{I}_{N\times N} \\ \mathbf{T} \\ -\mathbf{T} \end{bmatrix}; \mathbf{c} = \begin{bmatrix} \mathbf{l}\Delta u_{min} \\ -\mathbf{l}\Delta u_{max} \\ \mathbf{l}u_{max} - \mathbf{l}u(t-1) \\ -\mathbf{l}u_{min} + \mathbf{l}u(t-1) \end{bmatrix}.$$

where $\mathbf{I}_{N\times N}$ is the identity $N \times N$ matrix. Finally, the QP optimization problem can be stated as:

$$J(\mathbf{u}) = \frac{1}{2}\mathbf{u}^T\mathbf{H}\mathbf{u} + \mathbf{b}^T\mathbf{u} + \mathbf{f}_0$$

subject to:

$$\mathbf{R}\Delta\mathbf{u} \leqslant \mathbf{c}$$

where $\mathbf{H} = 2(\mathbf{G}^T\mathbf{G} + \lambda\mathbf{I})$, $\mathbf{b}^T = 2(\mathbf{f} - \mathbf{w})^T\mathbf{G}$, $\mathbf{f}_0 = (\mathbf{f} - \mathbf{w})^T(\mathbf{f} - \mathbf{w})$ and $\mathbf{w}$ is the vector of reference signals [27].

3.4. Tuning Procedure

In order to obtain the performance that satisfies the clinical requirements, all the tuning parameters need to be adjusted to handle the set-point following and disturbances rejection tasks. Usually, the effective disturbance rejection in GPC algorithm requires an aggressive tuning of the controller [37], which results in an undesired undershoot in the reference tracking performance. This requires to handle the set-point following and disturbance rejection tasks separately. Therefore, tuning is divided into two phases. Firstly, the GPC controller is tuned by considering also the F_d filter and introducing the disturbance modelled as a two steps (one positive and the other negative) signal [18]. At this stage, the following parameters are obtained: N, N_u, λ, and T_d, which are, respectively, the prediction horizon, the control horizon, the control signal weighing factor and the F_d filter time constant.

Following the same approach of [11, 17], the tuning is performed with a genetic algorithm (with 40 elements of initial population generated with a uniform distribution and with a Gaussian mutation function) that minimizes the worst-case integrated absolute error (IAE) for a dataset of 13 patients. This dataset has been proposed in [7, 17, 25] and it is representative of a wide population. The corresponding model parameters are shown in Table 1. The IAE is defined as:

$$IAE = \int |r(t) - BIS(t)|dt. \tag{9}$$

Formally, the cost function to be minimized is defined as

$$\min_{N,N_u,\lambda,T_d} \max_{k\in\{1,\ldots,13\}} IAE_k(N, N_u, \lambda, T_d), \tag{10}$$

where $IAE_k(N, N_u, \lambda, T_d)$ denotes the IAE index obtained from the kth patient of the dataset. Then, the F_r filter time constant T_r is determined considering the already tuned GPC but focusing only on the set-point response. In this case too, the value of T_r is determined in order to minimize the worst-case IAE value in the set-point step response. With this approach the obtained tuning is optimized for a whole dataset (the 13 patients) rather than for

Id	Age	Height $[cm]$	Weight $[kg]$	Gender	$C_{e_{50}}$	γ	E_0	E_{max}
1	40	163	54	F	6.33	2.24	98.8	94.10
2	36	163	50	F	6.76	4.29	98.6	86.00
3	28	164	52	F	8.44	4.10	91.2	80.70
4	50	163	83	F	6.44	2.18	95.9	102.00
5	28	164	60	M	4.93	2.46	94.7	85.30
6	43	163	59	F	12.00	2.42	90.2	147.00
7	37	187	75	M	8.02	2.10	92.0	104.00
8	38	174	80	F	6.56	4.12	95.5	76.40
9	41	170	70	F	6.15	6.89	89.2	63.80
10	37	167	58	F	13.70	1.65	83.1	151.00
11	42	179	78	M	4.82	1.85	91.8	77.90
12	34	172	58	F	4.95	1.84	96.2	90.80
13	38	169	65	F	7.42	3.00	93.1	96.58

Table 1: Patient database for propofol infusion models.

specific one. In this way the resulting tuning provides a better response of the control system to patient variability.

The controller parameters obtained from the optimization procedure are shown in Table 2.

N	27
N_u	7
λ	1.6
T_d	22.7
T_r	22.4

Table 2: Tuning parameters for the propofol infusion in DoH control system.

4. Simulation results

The control system evaluation is performed for the induction and the maintenance phases focusing on the medical specifications fulfilment and by comparing the results, using specific performance indexes, with those obtained by controllers already proposed in the literature. Moreover, the robustness analysis with respect to the inter- and the intra-patient variability is shown. Finally, the developed predictive control structure is evaluated with different disturbance scenarios, representing typical surgical stimuli.

The controller performance is first analyzed by considering the response of the proposed scheme to the set-point change from the initial BIS value to the desired hypnosis level of BIS=50. Additionally, a two steps disturbance is also applied to mimic the surgical stimuli that affects the DoH level. This analysis is initially performed for the representative population of patients in Table 1. As a first illustrative example, patient 13 is selected. The patient is characterized by the following linear model:

$$PK(s) = \frac{0.2342s^2 + 0.001631s + 1.521 \cdot 10^{-6}}{s^3 + 0.02404s^2 + 9.904 \cdot 10^{-5}s + 4.726 \cdot 10^{-8}} \tag{11}$$

$$PD(s) = \frac{0.00765}{s + 0.00765} \tag{12}$$

which is connected in series with the nonlinear Hill function

$$BIS(t) = 93.1 - 96.58 \left(\frac{C_e(t)}{C_e(t) + 7.42} \right)^3 \tag{13}$$

Note that, since the Hill function parameters are not known and its average values are employed (see subsection 3.2), there is a mismatch in the nonlinear element of the model that is used in the external predictor and the one that represents the virtual patient. Results are shown in Figure 3. It is noticeable that the performance achieved meets all the clinical requirements. In fact, the BIS level attains the set-point reference without undershoot and within the desired settling time. In order to provide a more exhaustive evaluation, we use the performance indexes proposed in [25]. For the set-point following (the induction phase) task we have:

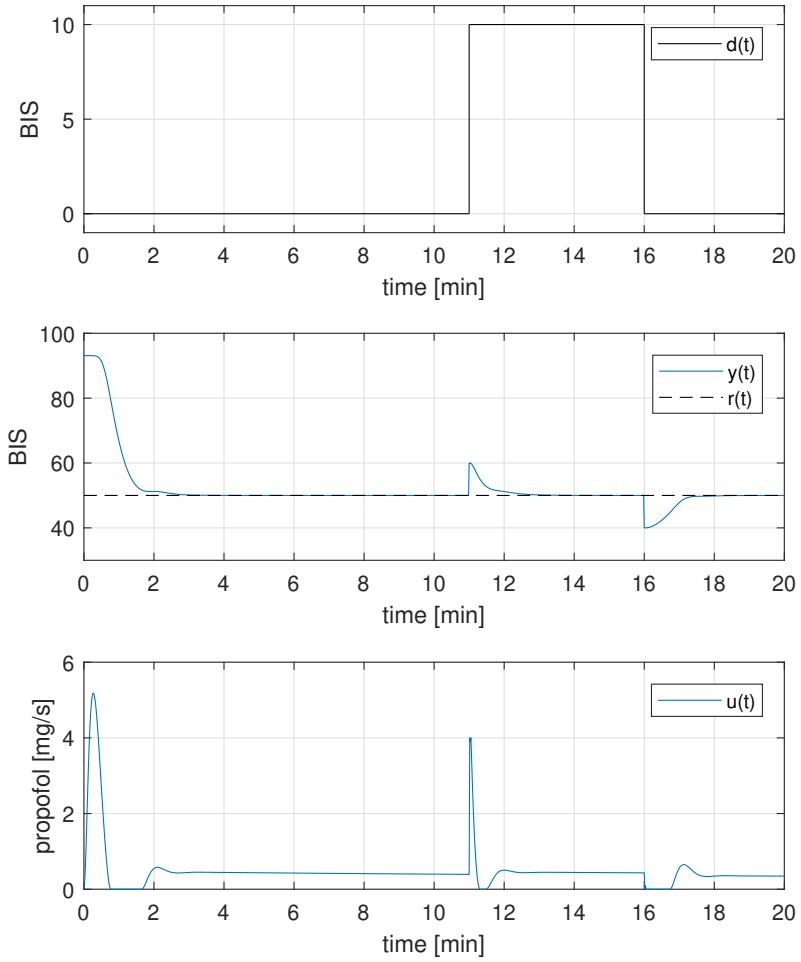

Fig. 3: Results for the average patient 13 using the proposed control system.

- TT: observed time-to-target (in minuts) required for reaching the first time the target interval of $[45 \div 55]$ BIS values;
- BIS-NADIR: the lowest observed BIS value;
- ST10: settling time, defined as the time interval for the BIS to reach and steady within the BIS range between 45 and 55 (that is, the target value of 50 ± 5);
- ST20: the same of ST10 but it considers a BIS range of 40 and 60;
- US: undershoot, defined as the difference between the lower threshold of 45 and the minimum value of BIS below this threshold.

From the disturbance rejection point of view, only the TT and the BIS-NADIR indexes are meaningful and they are calculated separately for the positive and for the negative step, represented as 'p' and 'n' sub-indexes.

The numerical performance evaluation for the average patient is shown in Table 3. In this case, the TT is equal to the ST10 index, which means that the BIS signal does not exceed the 45 and 55 thresholds and BIS-NADIR indicates no undershoot. Considering the disturbance rejection task, during the maintenance phase, it is possible to see that the control action increases to compensate the first (positive) step in order to decrease the DoH of the patient and vice versa with the second (negative) step. The controller response for this task is much more aggressive compared to the set-point tracking one (see Figure 3), because a fast rejection of the disturbances is required. The indexes for each disturbance step are summarized in Table 4. The settling times TTn and TTp meet the clinical

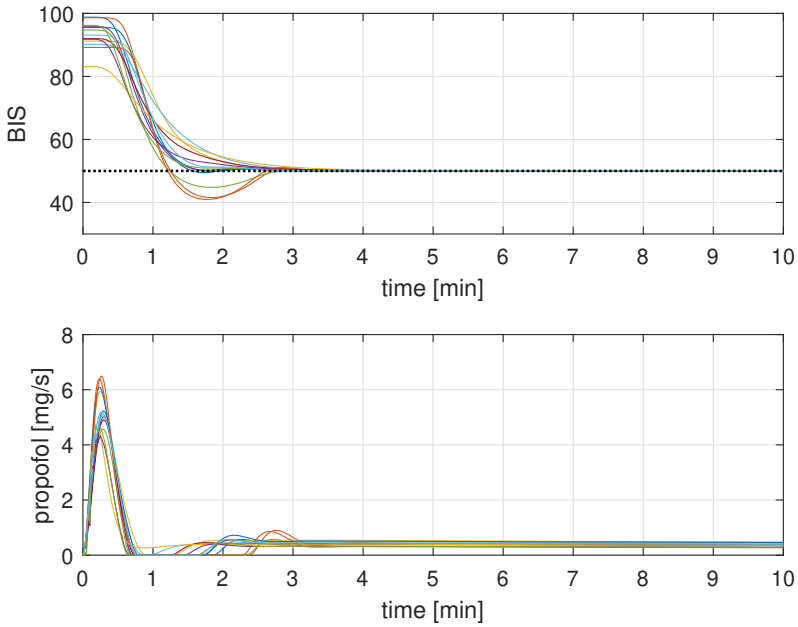

Fig. 4: BIS level and control action in the induction phase for each patient.

practice requirements, since the controller action yields a fast disturbance rejection without excessive overshoot in the BIS level, as proved by BIS-NADIRp and BIS-NADIRn. The TTn value is higher than TTp because of the lower saturation limit of the pump. In fact, when a negative step disturbance occurs, the controller has to decrease the infusion in order to increase the DOH of the patient, but the lower infusion limit is zero. Therefore, the BIS level increases naturally, which implies a higher settling time.

TT $[min]$	**BIS-NADIR**	**ST20** $[min]$	**ST10** $[min]$	**US**
1.37	50.00	1.18	1.37	0.00

Table 3: Performance indexes for the induction phase for the average patient 13.

TTp $[min]$	**BIS-NADIRp**	**TTn** $[min]$	**BIS-NADIRn**
0.33	50.00	0.78	50.00

Table 4: Performance indexes for the maintenance phase for the average patient 13.

4.1. Robustness analysis

Robustness is a very critical issue in anesthesia control and it should especially be analyzed for MPC approaches because model uncertainties can result in a significant performance deterioration or event instability.

In order to validate the robustness to inter-patient variability, the same tests performed on the average patient 13 have been repeated for all the patients in Table 1. Note that, also in these tests, the hypothesis of perfect knowledge of the linear part of the process model is applied ($\tilde{P} = P$) but the average Hill function is used in the controller instead of the actual patient's one ($\tilde{H} \neq H$). The process outputs and the control actions for the induction phase are shown in Figure 4. It can be observed that the BIS signals are very similar: all the patients enter the BIS [60-40] range in the required time interval (about 100 $[s]$) and all settle at the established reference in comparable times. The transient responses are very similar.

The performance indexes for the analyzed cases are shown in Table 5, and they are referred to as "A". They are compared with the results obtained with the model-based PID control scheme presented in [17], which is referred to in Table 5 as scheme "B". From the comparison, it appears that the MPC system outperforms the PID-based control system, obtaining lower values of TT, TS10 and TS20, which implies a faster response. For example, the

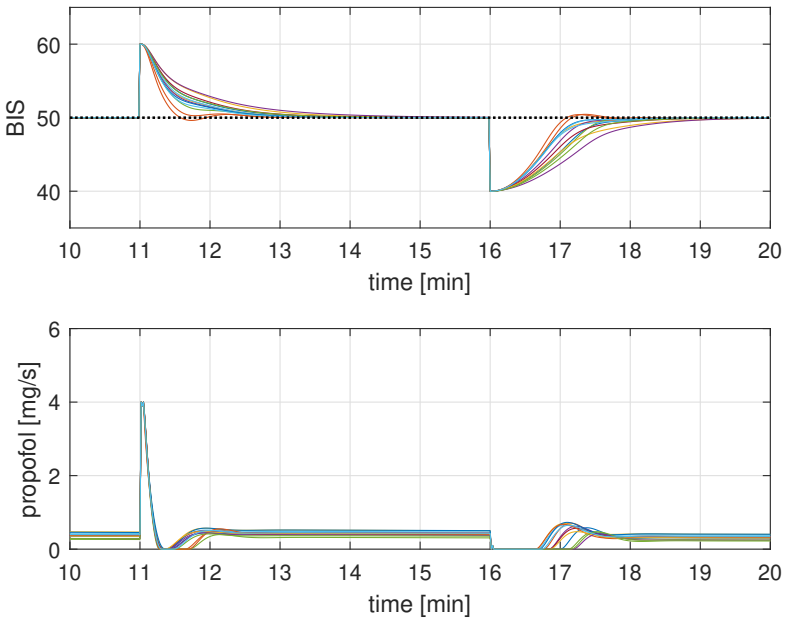

Fig. 5: BIS level and control action in the maintenance phase for each patient.

MPC-based scheme improves the average value of TT of about 21% with respect to the PID-based scheme. In addition, the average BIS-NADIR value is 48.22 with standard deviation of 3.38, which is comparable with the PID-based controller.

Then, the proposed approach has been compared with previously developed MPC systems. In particular, we consider the methods presented in [25] and [7], since both use the same evaluation dataset of Table 1. In [25] the reported results for the MPC control strategy (in this case the EPSAC algorithm is used) show an average settling time (TT index) of 1.8 min, which is 28% larger than the average TT obtained by the approach proposed in this paper. In addition, the ST10 index reported in [25] has a value of 2.05 min, in contrast to 1.66 minutes obtained by the control scheme proposed here, with an average BIS-NADIR index of 48.06. Finally, the average settling time (analog to the ST10 index) reported in [7] is around 4 minutes, which is higher than the one obtained with the proposed method.

The control system robustness to inter-patient variability is also verified for the disturbance rejection test. In Figure 5 the response to the disturbances is shown for each patient, while the corresponding performance indexes are shown in Table 6. The obtained results meet all the clinical requirements. Comparing the obtained results with those reported in [17], it can be seen that both control systems have a similar performance for the positive disturbance step. However, the situation changes when the negative disturbance step occurs. In this case the proposed control scheme is significantly faster (about 25%) than the PID-based scheme, yet it obtains similar overshoot values.

The same tests have also been executed on 500 patients generated by applying a Monte Carlo method (MCM) to validate further the controller robustness to the inter-patient variability, as done in [17]. The patient models are generated selecting randomly the gender, and considering a uniform distribution of the age between 18 and 70, of the height between 150 $[cm]$ and 190 $[cm]$, and of the weight between 50 $[kg]$ and 100 $[kg]$. Then, the distribution of the values for the Hill function parameters has been taken from [31,32]. As in the previous case, P is fixed equal to $\tilde{P}$ and $\tilde{H}$ is chosen as the average Hill function. The results of the induction phase are shown in Figure 6, while those of the maintenance phase are shown in Figure 7. The corresponding indexes are shown in Tables 7 and 8. We note that two patients have an undershoot that exceeds the lower limit of 40. The problem is not relevant, as the excessive undershoot is minimal, reaching a BIS of 38 and 39 respectively.

The simulated results show that the control system is robust with respect to the inter-patient variability and the clinical specifications are always met.

In the previous tests a perfect knowledge of the linear part of the patient model has been assumed, because the objective was to test the robustness of the controller over a wide population. We also want to test the robustness of the controller against the mismatches of the linear part of the model, that is, against intra-patient variability. To this end, we consider the statistical distribution of the PK/PD model parameters reported in [31]. In particular,

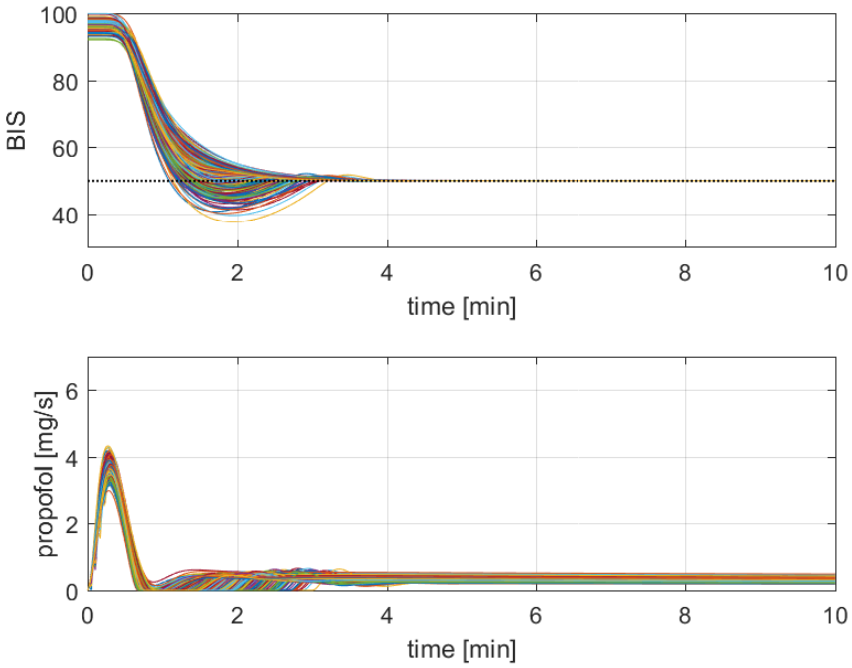

Fig. 6: Set-point step responses by using MCM for inter-patient variability.

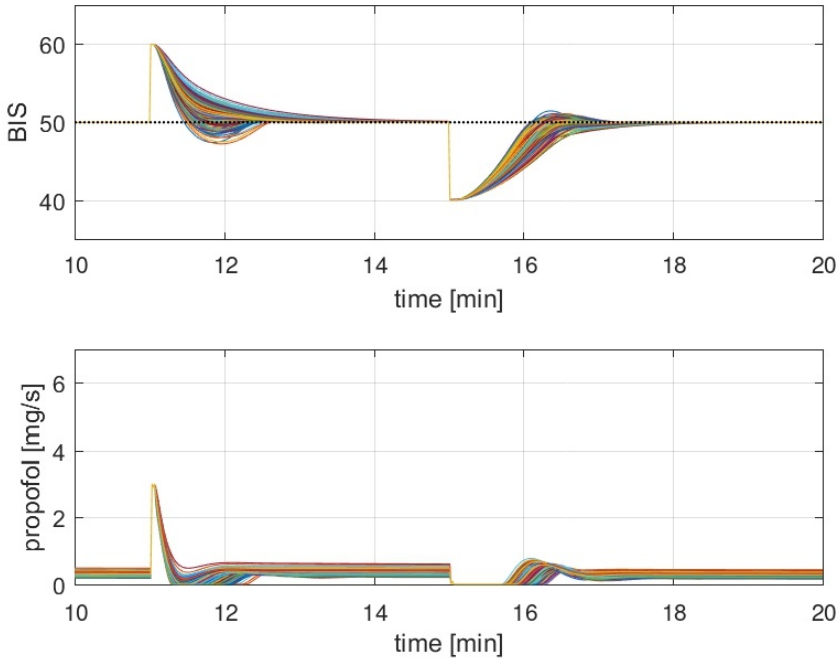

Fig. 7: Load disturbance responses by using MCM for inter-patient variability.

Patient	Scheme	TT [*min*]	BIS-NADIR	ST20 [*min*]	ST10 [*min*]	US
1	A	1.27	49.89	1.08	1.27	0.00
	B	1.63	49.55	1.32	1.63	0.00
2	A	1.15	41.60	1.05	2.33	3.40
	B	1.38	48.29	1.25	1.38	0.00
3	A	1.75	50.00	1.40	1.75	0.00
	B	2.01	49.90	1.70	2.01	0.00
4	A	1.25	50.00	1.29	1.25	0.00
	B	1.60	49.72	1.07	1.60	0.00
5	A	1.07	44.86	0.95	1.95	0.14
	B	1.33	49.20	1.09	1.33	0.00
6	A	1.90	50.00	1.50	1.90	0.00
	B	2.21	49.91	1.80	2.21	0.00
7	A	1.68	50.00	1.27	1.68	0.00
	B	1.96	49.76	1.54	1.96	0.00
8	A	1.27	49.51	1.12	1.27	0.00
	B	1.60	49.88	1.37	1.60	0.00
9	A	1.12	41.01	1.05	2.28	3.99
	B	1.33	44.71	1.23	2.01	0.29
10	A	1.92	50.00	1.38	1.92	0.00
	B	2.30	49.89	1.68	2.30	0.00
11	A	1.35	50.00	1.03	1.35	0.00
	B	1.65	49.54	1.22	1.65	0.00
12	A	1.20	50.00	0.98	1.20	0.00
	B	1.48	49.44	1.14	1.48	0.00
13	A	1.37	50.00	1.18	1.37	0.00
	B	1.72	49.75	1.44	1.72	0.00
mean	A	1.41	48.22	1.16	1.66	0.58
	B	1.71	49.19	1.39	1.76	0.03
std.dev	A	0.30	3.38	0.17	0.40	1.39
	B	0.42	1.99	0.23	0.30	0.08
max	A	1.92	50.00	1.50	2.33	3.99
	B	2.30	49.91	1.80	2.30	0.29
min	A	1.07	41.01	0.95	1.20	0.00
	B	1.33	44.71	1.09	1.33	0.00

Table 5: Performance indexes for the induction phase for each patient, where A is the proposed MPC-based control system, and B is the PID-based control system from [17].

for each patient of Table 1, $\tilde{P}$ is calculated basing on the average parameters values and P is generated by applying another MCM on the parameters using statistical distribution. For each patient, a set of 500 models has been generated. The responses of the average patient 13 for the induction phase are shown in Figure 8 and the corresponding performance indexes are summarized in Table 9. Despite the intra-patient variability, the set-point response is always satisfactory and the clinical specifications are always met. The results of this study, considering all the other patients, can be seen in Figure 9. The results of the maintenance phase of the average patient 13 are shown in Figure 10 and the performance indexes are shown in Table 10, while the results of all the patients are shown in Figure 11. It appears that the specifications are also met in the presence of intra-patient variability.

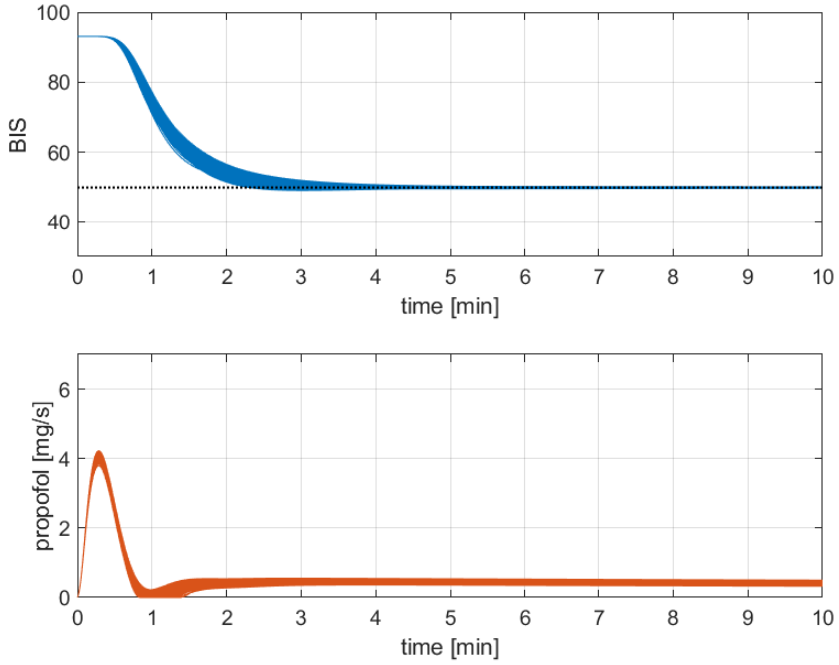

Fig. 8: Set-point step responses for intra-patient robustness (average patient 13).

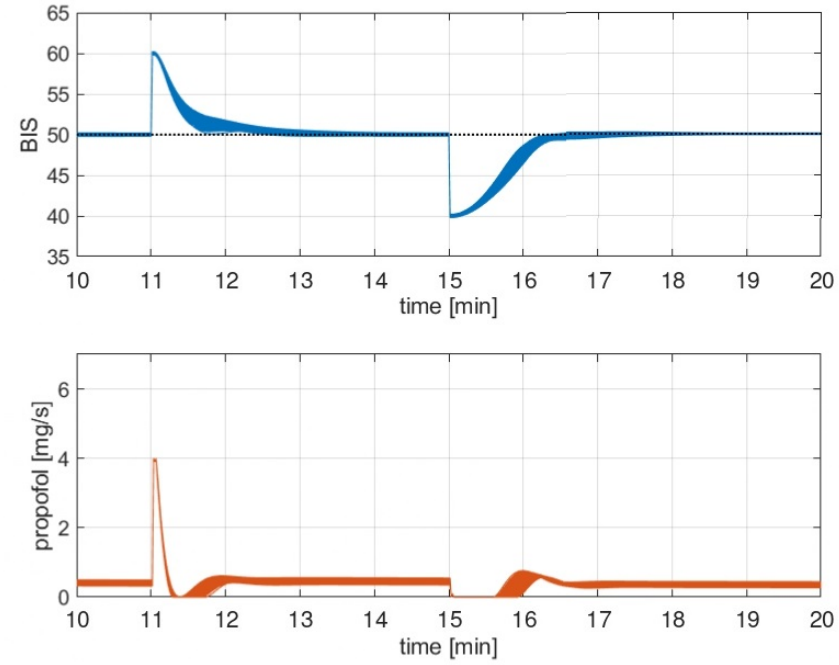

Fig. 9: Load disturbance responses for intra-patient robustness (average patient 13).

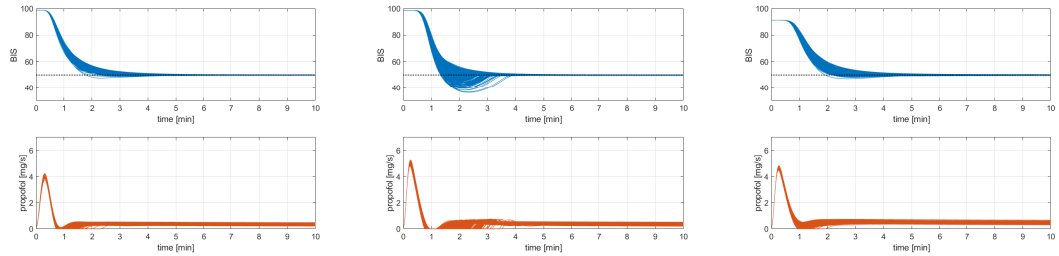

(a) Patient 1

(b) Patient 2

(c) Patient 3

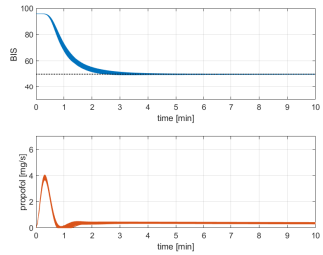

(d) Patient 4

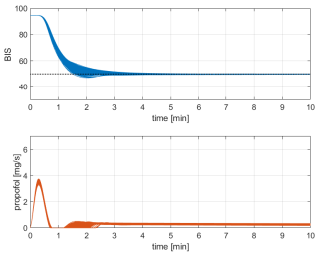

(e) Patient 5

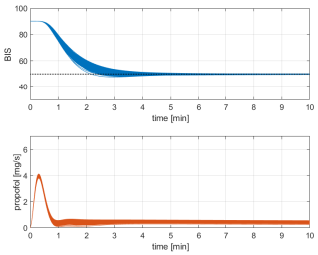

(f) Patient 6

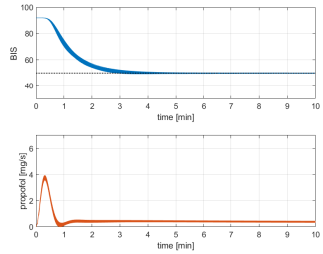

(g) Patient 7

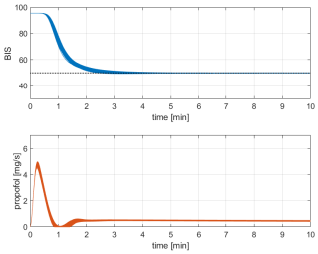

(h) Patient 8

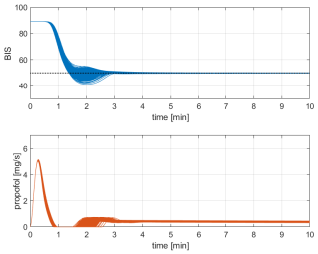

(i) Patient 9

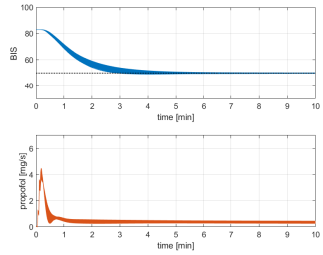

(j) Patient 10

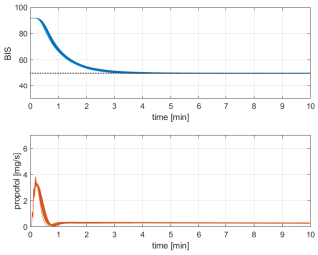

(k) Patient 11

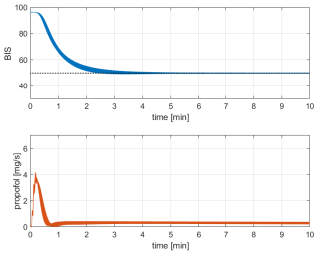

(l) Patient 12

Fig. 10: MCM results for the set-point step response for all patients.

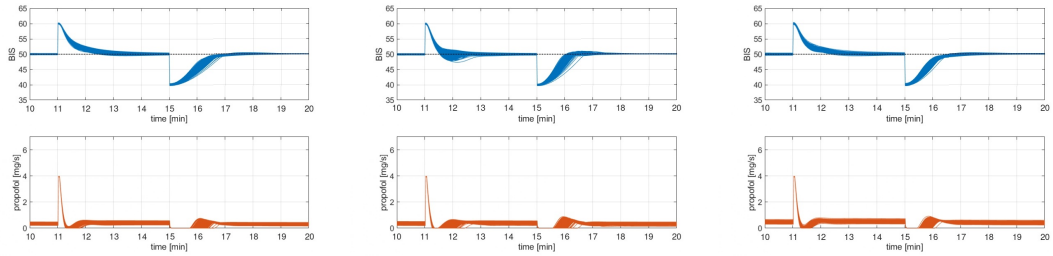

(a) Patient 1

(b) Patient 2

(c) Patient 3

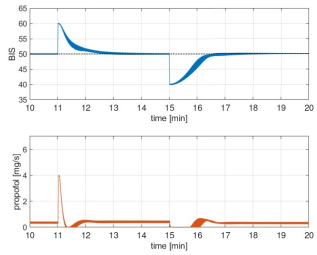

(d) Patient 4

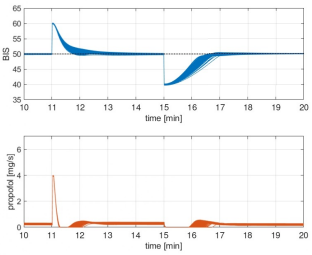

(e) Patient 5

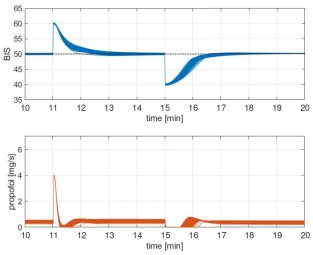

(f) Patient 6

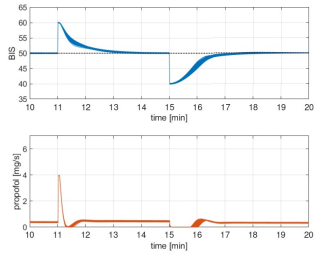

(g) Patient 7

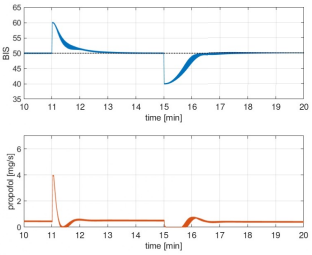

(h) Patient 8

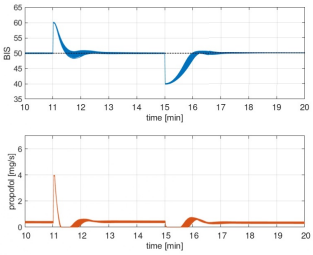

(i) Patient 9

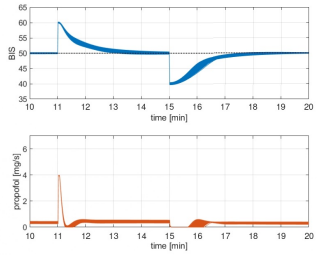

(j) Patient 10

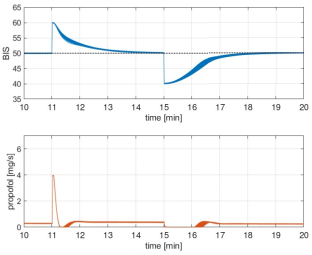

(k) Patient 11

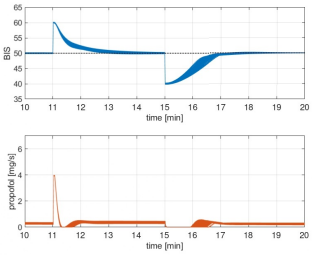

(l) Patient 12

Fig. 11: MCM results for the load disturbance response for all patients.

Patient	Patient	TTp [*min*]	BIS-NADIRp	TTn [*min*]	BIS-NADIRn
1	A	0.40	50.00	0.98	49.99
	B	0.42	50.02	1.26	50.03
2	A	0.28	50.00	0.75	50.46
	B	0.29	49.84	0.97	50.08
3	A	0.37	50.00	0.77	50.00
	B	0.39	50.02	1.00	50.05
4	A	0.37	50.00	0.85	50.00
	B	0.38	50.01	1.00	50.05
5	A	0.33	50.00	1.02	50.00
	B	0.36	50.00	1.37	50.03
6	A	0.38	50.00	0.77	49.99
	B	0.41	50.02	0.97	50.05
7	A	0.42	50.01	0.92	49.98
	B	0.45	50.02	1.15	50.03
8	A	0.33	50.00	0.78	50.00
	B	0.36	50.02	0.93	50.06
9	A	0.27	49.63	0.70	50.42
	B	0.28	50.02	0.86	50.08
10	A	0.50	50.02	0.98	49.93
	B	0.53	50.02	1.24	50.02
11	A	0.50	50.05	1.22	49.93
	B	0.53	50.01	1.53	50.00
12	A	0.40	50.01	1.08	49.99
	B	0.43	50.00	1.38	50.02
13	A	0.33	50.00	0.78	50.00
	B	0.36	50.02	0.97	50.06
mean	A	0.38	49.98	0.89	50.05
	B	0.40	50.00	1.12	50.04
std.dev	A	0.07	0.10	0.16	0.17
	B	0.08	0.05	0.21	0.02
max	A	0.50	50.05	1.22	50.46
	B	0.53	50.02	1.52	50.08
min	A	0.27	49.63	0.70	49.93
	B	0.28	49.84	0.86	50.00

Table 6: Performance indexes for the maintenance phase for each patient, where A is the proposed MPC-based control system, and B is the PID-based control system from [17].

	TT [*min*]	BIS NADIR	ST10 [*min*]	ST20 [*min*]	US
mean	1.46	49.16	1.18	1.51	0.12
std dev	0.21	1.91	0.13	0.29	0.66
min	0.98	37.64	0.88	1.08	0.00
max	2.03	50.00	2.43	2.87	7.36

Table 7: Performance indexes for the set-point tracking task with the MCM for inter-patient variability.

	TTp	BIS-NADIRp	TTn	BIS-NADIRn
mean	0.37	49.91	0.89	50.21
std.dev	0.05	0.34	0.08	0.26
max	0.25	47.24	0.70	50.00
min	0.60	50.00	1.13	51.45

Table 8: Performance indexes for the load disturbance rejection task with the MCM for inter-patient variability.

	TT [*min*]	**BIS-NADIR**	**ST20** [*min*]	**ST10** [*min*]	**US**
mean	1.40	49.57	1.17	1.39	0.00
std.dev	0.11	0.88	0.05	0.12	0.04
min	1.17	44.10	1.02	1.15	0.00
max	1.90	50.21	1.40	2.17	0.90

Table 9: Performance indexes for the set-point tracking task with the MCM for intra-patient variability (average patient 13).

	TTp [*min*]	**BIS-NADIRp**	**TTn** [*min*]	**BIS-NADIRn**
mean	0.39	49.98	0.78	50.04
std.dev	0.02	0.07	0.04	0.05
min	0.33	49.74	0.67	49.93
max	0.45	50.20	0.90	50.31

Table 10: Performance indexes for the load disturbance rejection task with the MCM for intra-patient variability (average patient 13).

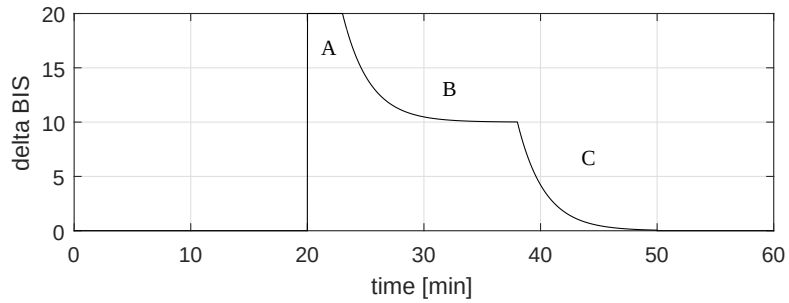

Fig. 12: Disturbance profile *I*:(A) arousal reflex due to the first surgical incision; (B) offset slowly decreases but settles at on onset of 10% due to continuous normal surgical stimuli; (C) withdrawal of stimuli during skin-closing.

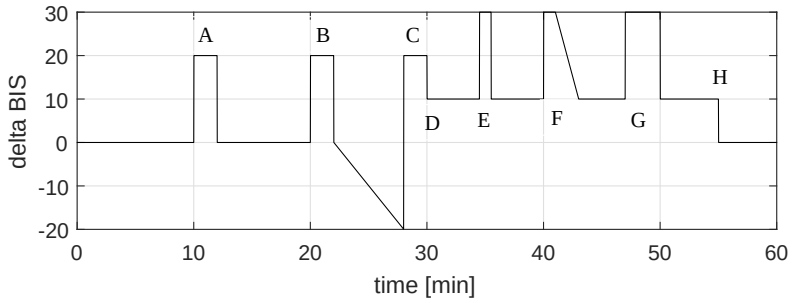

Fig. 13: Disturbance profile *II*: (A) laryngoscopy/intubation; (B) surgical incision followed by no surgical stimulation; (C) abrupt stimulus after a period of low stimulation; (D) onset of a continuous normal surgical stimulation; (E-G) stimulate short-lasting, larger stimuli; (H) withdrawal of stimuli during closing.

4.2. Surgical stimuli

The proposed method has also been evaluated with two different disturbance profiles, denoted as *I* and *II*, which have been previously used, respectively, in [12, 15] and [4, 7, 8]. They are shown in Figures 12 and 13.

Analyzing the results obtained with the disturbance profile *I* (see Figure 14), it is possible to observe that the controller provides a fast disturbance rejection as the BIS remains for a most of time at the desired level. Indeed, the BIS begins to reach the reference immediately after the step disturbance (A). The same happens for the last part (C) of the disturbance profile, resulting in a very small undershoot.

The results with the disturbance profile *II* are shown in Figure 15. In this case too the proposed control scheme obtains satisfactory results, handling properly all surgical stimuli. Note that the stage *C* in this disturbance profile provides a very challenging situation for the controller, since the absolute change in the disturbance is equal to 40. However, the proposed control system reacts very quickly and does not allow the BIS signal to exceed the set-point plus disturbance value. With these test scenarios it is confirmed that the proposed control system provides a reliable and robust solution for the DoH control in the anaesthesia process.

4.3. Computational aspects

All simulations have been performed in Matlab 2017a on a 64-bit PC platform (Intel i7 2.4 GHZ, 8 GB RAM) running Microsoft Windows 10. The formulated optimization problem has been solved online using classical QP from Matlab Optimization Toolbox. The average computational time required for the control signal calculation is 19 milliseconds.

5. Conclusions

We have presented a new MPC methodology for DoH control that uses the compensation of the nonlinear part of the process and an external predictor to fully exploit a GPC algorithm, based on an individualized patient model, where saturation and slew rate constraints of the control signal are taken into account. The tuning procedure of the overall control scheme has been performed using genetic algorithms and considering a dataset of patients representative of a wide population. The developed control structure is characterized by low complexity and low computational effort, so that it can be easily deployed to standard hardware and software platforms. The control

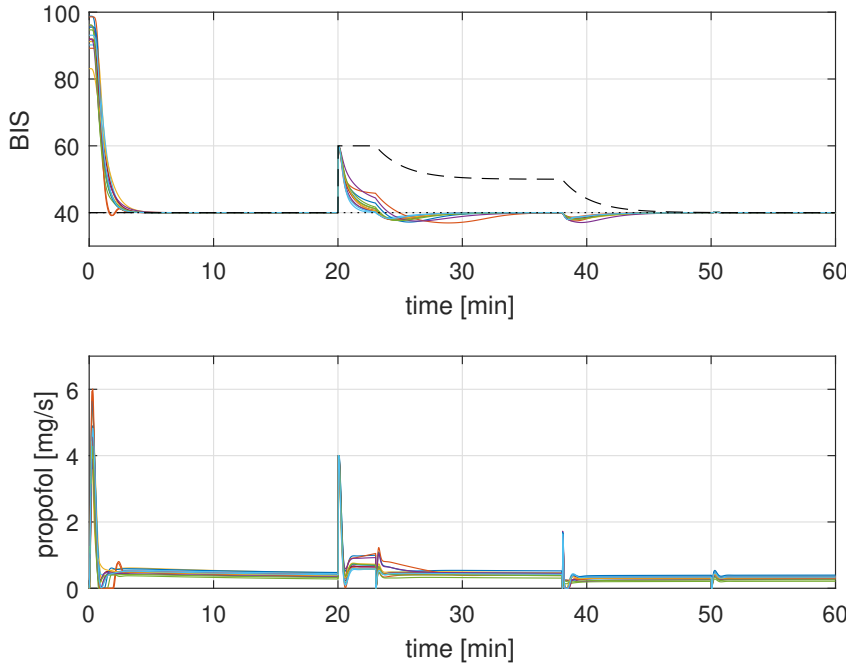

Fig. 14: Control system responses for disturbances profile *I* considering all 13 patients.

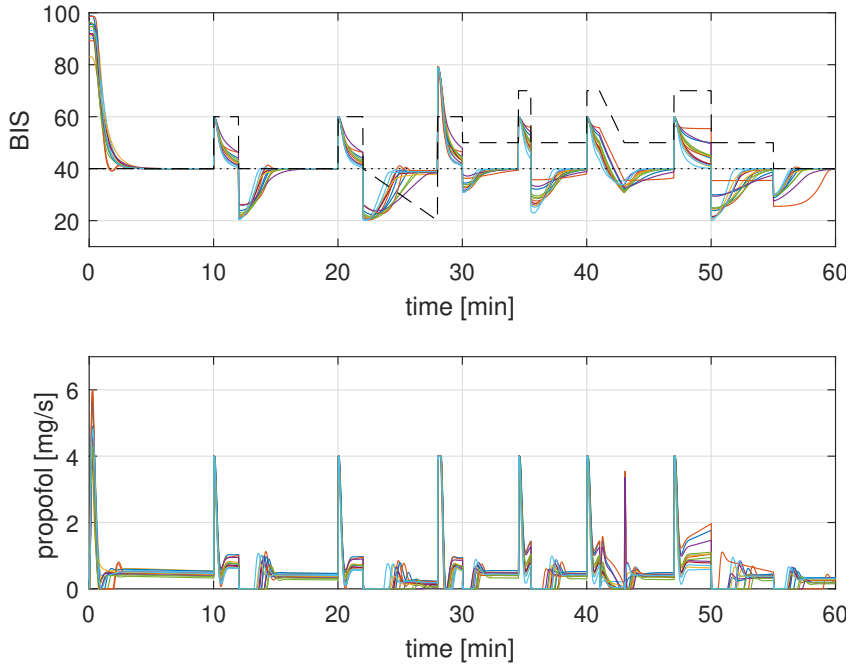

Fig. 15: Control system responses for disturbances profile *II* considering all 13 patients.

system has been tested through an extensive simulation study, considering inter- and intra-patient variability and by comparing it with other control schemes previously presented in the literature. The obtained results show that this new MPC approach provides a satisfactory performance for this challenging process.

Future work will be focused on the practical evaluation of the proposed control scheme during real clinical experiments. Such an evaluation will allow the assessment of the performance of the analyzed controller during typical surgical intervention and it will show its practical viability.

Acknowledgment

This work has been supported by EU–H2020 funds under MSCA Individual Fellowship - ACTAN project ID: 837912. Authors would like to thank Paolo Visieri for his help with control system simulations and performance indexes computation.

References

1. S. Ntouskas, H. Sarimveis, A robust model predictive control framework for the regulation of anesthesia process with propofol, Optimal Control Applications and Methods 42 (4) (2021) 965–986.
2. J. M. Bailey, W. M. Haddad, Drug dosing control in clinical pharmacology, IEEE Control Systems Magazine 25 (2) (2005) 35–51.
3. K. Lunze, T. Singh, M. Walter, M. Brendel, S. Leonhardt, Blood glucose control algorithms for type 1 diabetic patients: A methodological review, Biomedical Signal Processing and Control 8 (2) (2013) 107–119.
4. M. J. Khodaei, N. Candelino, A. Mehrvarz, N. Jalili, Physiological closed-loop control (PCLC) systems: Review of a modern frontier in automation, IEEE Access 8 (2020) 23965–24005.
5. C. Ionescu, M. Neckebroek, M. Ghita, D. Copot, An open source patient simulator for design and evaluation of computer based multiple drug dosing control for anesthetic and hemodynamic variables, IEEE Access 9 (2021) 8680–8694.
6. F. Padula, C. Ionescu, N. Latronico, M. Paltenghi, A. Visioli, G. Vivacqua, Inversion-based propofol dosing for intravenous induction of hypnosis, Communications in Nonlinear Science and Numerical Simulation 39 (2016) 481–494.
7. I. Nascu, R. Oberdieck, E. N. Pistikopoulos, Explicit hybrid model predictive control strategies for intravenous anaesthesia, Computers and Chemical Engineering 106 (2017) 814–825.
8. I. Nascu, E. N. Pistikopoulos, Modeling, estimation and control of the anaesthesia process, Computers and Chemical Engineering 107 (2017) 318–332.
9. B. Wayne-Bequette, Process control practice and education: Past, present and future, Computers and Chemical Engineering 128 (2019) 538–556.
10. A. R. Absalom, N. Sutcliffe, G. N. Kenny, Closed-loop control of anesthesia using bispectral index: Performance assessment in patients undergoing major orthopedic surgery under combined general and regional anesthesia, Anesthesiology 96 (1) (2002) 67–73.
11. F. Padula, C. Ionescu, N. Latronico, M. Paltenghi, A. Visioli, G. Vivacqua, Optimized PID control of depth of hypnosis in anesthesia, Computer Methods and Programs in Biomedicine 144 (2017) 21–35.
12. G. A. Dumont, A. Martinez, J. M. Ansermino, Robust control of depth of anesthesia, International Journal of Adaptive Control and Signal Processing 23 (2009) 435–454.
13. K. Soltesz, J.-O. Hahn, T. Hägglund, G. A. Dumont, J. M. Ansermino, Individualized closed-loop control of propofol anesthesia: A preliminary study, Biomedical Signal Processing and Control 8 (6) (2013) 500–508.
14. K. Soltesz, K. van Heusden, M. Hast, J. M. Ansermino, G. A. Dumont, A synthesis method for automatic handling of inter-patient variability in closed-loop anesthesia, Proceedings of the American Control Conference, Boston, USA.
15. J.-O. Hahn, G. A. Dumont, J. M. Ansermino, Robust closed-loop control of hypnosis with propofol using wav_{CNS} index as the controlled variable, Biomedical Signal Processing and Control 7 (5) (2012) 517–524.
16. T. D. Smet, M. M. R. F. Struys, S. Greenwald, E. P. Mortier, S. L. Shafer, Estimation of optimal modeling weights for a bayesian based closed loop system for propofol administration using the bispectral index as a controlled variable: A simulation study, Anesthesia & Analgesia 105 (2007) 1629–1638.
17. L. Merigo, F. Padula, A. Pawlowski, S. Dormido, J. L. Guzman, N. Latronico, M. Paltenghi, A. Visioli, A model-based control scheme for depth of hypnosis in anesthesia, Biomedical Signal Processing and Control 42 (2018) 216–229.
18. A. Pawlowski, L. Merigo, J. Guzmán, S. Dormido, A. Visioli, Two-degree-of-freedom control scheme for depth of hypnosis in anesthesia, IFAC-PapersOnLine 51 (4) (2018) 72–77.
19. J. A. Reboso, J. M. Gonzalez-Cava, A. Leon, J. A. Mendez-Perez, Closed loop administration of propofol based on a Smith predictor: a randomized controlled trial, Minerva anestesiologica 85 (6) (2018) 585–593.
20. T. Mendonça, J. Lemos, H. Magalhães, P. Rocha, S. Esteves, Drug delivery for neuromuscular blockade with supervised multimodel adaptive control, IEEE Transactions on Control System Technology 17 (6) (2009) 1237–1244.
21. M. Schiavo, L. Consolini, M. Laurini, N. Latronico, M. Paltenghi, A. Visioli, Optimized feedforward control of propofol for induction of hypnosis in general anesthesia, Biomedical Signal Processing and Control 66 (2021) 102476.
22. A. Krieger, E. N. Pistikopoulos, Model predictive control of anesthesia under uncertainty, Computers and Chemical Engineering 71 (2014) 699–707.

23. I. Nascu, R. Oberdieck, E. N. Pistikopoulos, An explicit hybrid model predictive control strategy for intravenous anaesthesia, Proceedings of the 9th IFAC Symposium on Biological and Medical Systems BMS, Berlin, Germany.
24. H. Chang, A. Krieger, A. Astolfi, E. Pistikopoulos, Robust multi-parametric model predictive control for LPV systems with application to anaesthesia, Journal of Process Control 44 (10) (2014) 1538–1547.
25. C. M. Ionescu, R. D. Keyser, B. C. Torrico, T. D. Smet, M. M. Struys, J. E. Normey-Rico, Robust predictive control strategy applied for propofol dosing using BIS as a controlled variable during anesthesia, IEEE Transactions on Biomedical Engineering 55 (9) (2008) 2161–2170.
26. Y. Sawaguchi, E. Furutani, G. Shirakami, M. Araki, K. Fukuda, A model-predictive hypnosis control system under total intravenous anesthesia, IEEE Transactions on Biomedical Engineering 55 (3) (2008) 874–887.
27. E. F. Camacho, C. Bordóns, Model Predictive Control, Springer-Verlag, London, UK, 2007.
28. A. Pawlowski, L. Merigo, J. L. Guzman, A. Visioli, S. Dormido, Event-based GPC for depth of hypnosis in anesthesia for efficient use of propofol, Proceedings of the 3rd International Conference on Event-Based Control, Communication and Signal Processing (EBCCSP), Funchal, Portugal.
29. D. Ingole, M. Kvasnica, FPGA implementation of explicit model predictive control for closed loop control of depth of anesthesia, Proceedings of the 5th IFAC Conference on Nonlinear Model Predictive Control, Seville, Spain.
30. T. W. Schinder, C. F. Minto, S. L. Shafer, P. L. Andersen, D. B. Goodale, E. J. Youngs, The influence of age on propofol paharmacodynamics, Anesthesiology 90 (1999) 1502–1516.
31. T. W. Schnider, C. F. Minto, P. L. Gambus, C. Andresen, D. B. Goodale, E. J. Youngs, The influence of method of administration and covariates on the pharmacokinetics of propofol in adult volunteers, Anesthesiology 88 (1998) 1170–1182.
32. A. L. G. Vanluchene, H. Vereecke, O. Thas, E. P. Mortier, S. L. Shafer, M. M. R. F. Struys, Spectral entropy as an electroencephalographic measure of anesthetic drug effect, Anesthesiology 101 (2004) 34–42.
33. M. M. R. F. Struys, H. Vereecke, A. Moerman, E. W. Jensen, D. Verhaeghen, N. D. Neve, Ability of the bispectral index, autoregressive modelling with exogenous input-derived auditory evoked potentials responsiveness during anesthesia with propofol and remifentanil, Anesthesiology 99 (2003) 802–812.
34. L. Merigo, F. Padula, N. Latronico, T. Mendonca, M. Paltenghi, P. Rocha, A. Visioli, On the identification of the propofol PK/PD model using BIS measurements, Proceedings of the 20th World Congress of the International Federation of Automatic Control, IFAC, Toulouse, France.
35. C. Ionescu, A computationally efficient hill curve adaptation strategy during continuous monitoring of dose-effect relation in anaesthesia, Nonlinear Dynamics 92 (3) (2018) 843—-852.
36. B. Marsh, M. White, N. Norton, G. N. Kenny, Pharmacokinetic model driven infusion of propofol in children, British Journal of anesthesia 67 (1991) 41–48.
37. A. Pawlowski, J. L. Guzmán, J. E. Normey-Rico, M. Berenguel, Improving feedforward disturbance compensation capabilities in generalized predictive control, Journal of Process Control 22 (3) (2012) 527–539.